

Sharp Kelvinlets: Elastic Deformations with Cusps and Localized Falloffs

Fernando de Goes
Pixar Animation Studios
fernando@pixar.com

Doug L. James
Pixar Animation Studios, Stanford University
djames@pixar.com



Figure 1: Comparison of incompressible Kelvinlet deformations generated using three vertical displacements with the same brush scale. Prior tri-scale Kelvinlet brush using multi-scale extrapolation (left) is inherently smooth, whereas our new Bi-Laplacian Kelvinlet solution (middle) can be blended with its Cusp Bi-Laplacian Kelvinlet counterpart (right) for increased control over brush sharpness and locality. ©Disney/Pixar

ABSTRACT

In this work, we present an extension of the regularized Kelvinlet technique suited to non-smooth, cusp-like edits. Our approach is based on a novel multi-scale convolution scheme that layers Kelvinlet deformations into a finite but spiky solution, thus offering physically based volume sculpting with sharp falloff profiles. We also show that the Laplacian operator provides a simple and effective way to achieve elastic displacements with fast far-field decay, thereby avoiding the need for multi-scale extrapolation. Finally, we combine the multi-scale convolution and Laplacian machinery to produce *Sharp Kelvinlets*, a new family of analytic fundamental solutions of linear elasticity with control over both the locality and the spikiness of the brush profile. Closed-form expressions and reference implementation are also provided.

CCS CONCEPTS

• Computing methodologies → Volumetric models.

KEYWORDS

Sculpting brushes, profile control, linear elasticity, regularized Kelvinlets.

ACM Reference Format:

Fernando de Goes and Doug L. James. 2019. Sharp Kelvinlets: Elastic Deformations with Cusps and Localized Falloffs. In *DigiPro '19: The Digital Production Symposium (DigiPro '19)*, July 27, 2019, Santa Barbara, CA, USA. ACM, New York, NY, USA, 8 pages. <https://doi.org/10.1145/3329715.3338884>

1 INTRODUCTION

Regularized Kelvinlets [de Goes and James 2017] provide analytical expressions for volume deformations based on regularized fundamental solutions of linear elastostatics in an infinite elastic

Permission to make digital or hard copies of part or all of this work for personal or classroom use is granted without fee provided that copies are not made or distributed for profit or commercial advantage and that copies bear this notice and the full citation on the first page. Copyrights for third-party components of this work must be honored. For all other uses, contact the owner/author(s).

DigiPro '19, July 27, 2019, Santa Barbara, CA, USA

© 2019 Copyright held by the owner/author(s).

ACM ISBN 978-1-4503-6799-8/19/07.

<https://doi.org/10.1145/3329715.3338884>

medium. Since their development and deployment in Pixar’s short *Lou* [Tieryas et al. 2017], these tools have been widely adopted both as a sculpting brush and as a rigging deformer. Figures 2 and 3 showcase some results produced using Kelvinlets in Pixar’s feature film *Incredibles 2* [Hamou-Lhadj et al. 2018] (see also the supplemental video). Despite the interactive physics-based response, Kelvinlet solutions offer no control on the sharpness of the brush profile, thus limiting cusped edits such as creases and spikes.

In this paper, we introduce an extended and more general collection of Kelvinlet deformations that provide fine control over both the sharpness and the spatial locality of the brush falloff. First, we derive a new solution of linear elastostatics that presents a cusp-like profile, which is achieved by convolving the original Kelvinlet displacements across various regularization scales using a kernel function and subject to finiteness constraints. We then show that elastic deformations with fast far-field decay can be computed by taking Laplacians of the Kelvinlet solutions. This approach leads to simpler closed-form expressions that have increasingly rapid decay upon repeated Laplacian differentiation. By combining these two techniques, we obtain physically based volume sculpting with cusped and localized falloffs, which we refer to as *Sharp Kelvinlets*.

2 RELATED WORK

Spiky falloff profiles are commonly used in geometric sculpting systems to provide precise editing of non-smooth details such as creases or cusps. However, similar to other non-physical modeling brushes, these geometric deformers do not produce deformations consistent with physical elasticity and thus offer limited compressibility and smoothness control. Sculpting brushes designed to produce incompressible flows [Angelidis et al. 2006, 2004; von Funck et al. 2006] are also insufficient to support cusp-like solutions. Similarly, the formulation of regularized Kelvinlets [de Goes and James 2017] involves only smooth deformations contingent to a regularization density function. In contrast, we present in this work spiky static solutions of linear elasticity.

Finite sharp solutions are rare in elastostatics, since distributed loads tend to produce smooth displacement profiles. Exceptions



Figure 2: Kelvinlet deformations in “Jack-Jack vs Raccoon” fight sequence: (Top) Input animation; (Middle) animation shot polishing was done using Kelvinlet sculpting brushes to achieve the desired deformations of Jack-Jack; (Bottom) final render. ©Disney/Pixar

occur in contact mechanics for nonsmooth indentors, e.g., the analytical solution due to a conical indenter contacting an elastic half-space has been derived for punch tools [Sneddon 1965]. In other fields, cusped solutions occur naturally for nonlinear dynamical systems described by specific partial differential equations. Examples include solutions for non-linear wave equations [Qiao and Qiao 2005], spiky features in pattern formation [Iron et al. 2001], or magnon solutions in string theory [Ishizeki and Kruczenski 2007], where their dynamic stability is of interest. We instead target the design of sharp falloffs associated with elastic deformations caused by static load. To our knowledge, our work is the first to produce finite and regularized cusp-like solutions to elastostatic equations.

Our approach takes inspiration from scale-space filtering techniques pioneered by Witkin [1983], which involve multi-scale Gaussian convolutions of signals to support scale-specific signal analysis, e.g., of images in computer vision [Sporring et al. 2013]. However, we use multi-scale convolution not for the analysis of arbitrary signals, but rather for the analytical derivation of elasticity solutions with specific spatial properties. A discrete version of multi-scale convolution was previously considered by de Goes and James [2017], which combined a finite number of Kelvinlet solutions with different scales to achieve faster far-field decay. Alternatively, we rely on Laplacian differentiation of Kelvinlets to obtain fast decay, and introduce continuous multi-scale convolution to obtain generalized closed-form elastic deformations with spiky profiles.

3 PRIMER ON REGULARIZED KELVINLETS

We begin by briefly summarizing the notation and formulation of regularized Kelvinlets [de Goes and James 2017]. We denote a point in 3D by \mathbf{r} , its norm by $r = \|\mathbf{r}\|$, and its regularized norm by $r_\epsilon = \sqrt{r^2 + \epsilon^2}$, where $\epsilon > 0$ is a radial regularization scale. We define a displacement field by $\mathbf{u}: \mathbb{R}^3 \rightarrow \mathbb{R}^3$ and its corresponding body load by $\mathbf{b}: \mathbb{R}^3 \rightarrow \mathbb{R}^3$. A displacement \mathbf{u} represents a solution to linear elastostatics in response to a load \mathbf{b} if and only if the Navier-Cauchy equation $\mathbf{N}\mathbf{u} = \mathbf{b}$ is verified [Slaughter 2002]. Here, we use \mathbf{N} as

short for the (linear) Navier’s operator:

$$\mathbf{N}\mathbf{u} = \mu\Delta\mathbf{u} + \frac{\mu}{(1-2\nu)}\nabla(\nabla\cdot\mathbf{u}), \quad (1)$$

which includes the elastic shear modulus $\mu > 0$ indicating the material stiffness, and the Poisson ratio $\nu \in [0, 1/2)$ controlling the volume compressibility. In the special case of $\nu = 1/2$, the displacement is hard constrained to be divergence-free (i.e., $\nabla\cdot\mathbf{u} = 0$), thus leading to an incompressible deformation.

Regularized Kelvinlets are solutions to linear elastostatics associated with a smoothed point load of the form $\mathbf{b}(\mathbf{r}) = \mathbf{f}\rho_\epsilon(\mathbf{r})$, where \mathbf{f} is a force vector and ρ_ϵ is a normalized density function. In [de Goes and James 2017], this density was set to the smooth radially symmetric function $\rho_\epsilon(r) = (15\epsilon^4)/(8\pi r_\epsilon^7)$. A regularized Kelvinlet can be encoded by a 3×3 matrix $\mathcal{K}_\epsilon(\mathbf{r})$ that maps a force vector \mathbf{f} to a displacement \mathbf{u}_ϵ at point \mathbf{r} . This solution can further be expanded into a canonical form:

$$\mathbf{u}_\epsilon(\mathbf{r}) = \mathcal{K}_\epsilon(\mathbf{r})\mathbf{f} = [A_\epsilon(r)\mathbf{I} + B_\epsilon(r)\mathbf{r}\mathbf{r}^\top]\mathbf{f}, \quad (2)$$

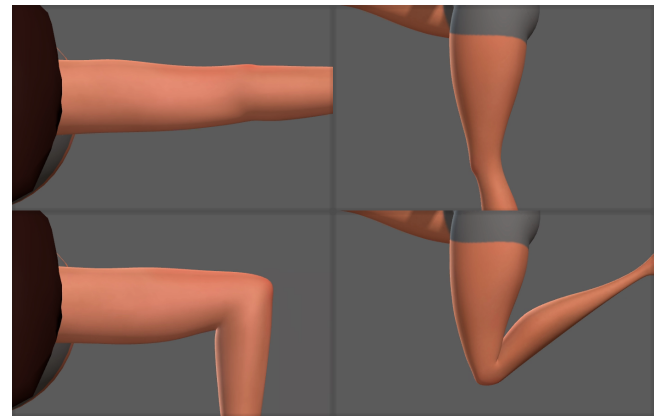


Figure 3: Rig muscle bulges were achieved using Kelvinlet de-formers, here shown for Helen from Incredibles 2. ©Disney/Pixar

with the radial scalar coefficients given analytically by

$$A_\varepsilon(r) = \frac{(a-b)}{r_\varepsilon} + \frac{a}{2} \frac{\varepsilon^2}{r_\varepsilon^3} \quad \text{and} \quad B_\varepsilon(r) = \frac{b}{r_\varepsilon^3}, \quad (3)$$

where $a = 1/(4\pi\mu)$ and $b = a/[4(1-\nu)]$.

Several extensions of the regularized Kelvinlet formulation were considered in [de Goes and James 2017, 2018], including a 2D solution, generalization to affine transformations, and an elastodynamic analogue. In particular, a multi-scale extrapolation scheme was proposed to control the displacement falloff profile. By combining a discrete number of Kelvinlets with varying scales, the far-field decay evaluated as $r \rightarrow \infty$ can be adjusted from $O(1/r)$ to high-order rates. For instance, the difference between two Kelvinlets reduces the brush decay to $O(1/r^3)$. In the next sections, we revisit the spatial locality of Kelvinlet solutions using differentiation and exploit multi-scale superposition to generate spiky deformations.

4 FALLOFF PROFILES

Falloff profiles are commonly used to define the influence of radially symmetric deformers (Figure 4), and typically control the amount of sharpness versus smoothness nearby the brush tip, as well as the decay rate at larger distances. For example, if we define a falloff profile as a function $P(r) \geq 0$ based on the radial distance $r \geq 0$, we can then define a radially symmetric displacement field $\mathbf{u}(\mathbf{r}) = P(r) \mathbf{u}_0$. This notion of sculpting profile does not immediately generalize to physics-based elastic deformers, such as regularized Kelvinlets, since the displacement field resulting from a (regularized) force load lacks radial symmetry for physical reasons, e.g., violation of compressibility constraints.

To analyze the falloff profile of Kelvinlet solutions, we find it useful to use a simplified deformation problem. We consider the x -component of the displacement field $\mathbf{u}_\varepsilon(\mathbf{r})$ resulting from a (regularized) unit load in the $+x$ direction applied at the origin. Since Kelvinlets are accompanied by the matrix $\mathcal{K}_\varepsilon(\mathbf{r})$, this specialized deformation problem corresponds to $\mathbf{u}_\varepsilon([x, 0, 0]) = \mathcal{K}_\varepsilon([x, 0, 0])[1, 0, 0]^\top$, and therefore its non-trivial solution reduces to the matrix entry $K_\varepsilon^{xx}([x, 0, 0])$. We thus define the Kelvinlet profile function as:

$$P(x) = K_\varepsilon^{xx}([x, 0, 0]) = A_\varepsilon(|x|) + B_\varepsilon(|x|)x^2. \quad (4)$$

Substituting (3) into (4), we obtain:

$$P(x) = \frac{a}{x_\varepsilon} + \frac{a\varepsilon^2}{2x_\varepsilon^3} - \frac{b\varepsilon^2}{x_\varepsilon^3}, \quad (5)$$

which is symmetric in x and has a clear $O(1/x)$ falloff as $|x| \rightarrow \infty$.

5 CUSPED KELVINLETS

In this section, we show how to construct a modified Kelvinlet solution with a spiky falloff, which we name *cusped Kelvinlet*. We define a cusp as a non-zero displacement with discontinuous derivative about the brush center. Our approach consists of designing a falloff profile that approximates a linear function $P(x) \approx P(0)(1 - |dx|)$ as $x \rightarrow 0$, where d is the desired slope parameter. Unfortunately, existing regularized Kelvinlets and multi-scale variants are inherently smooth and have zero gradients at the origin. This is observed by expanding the Kelvinlet profile function (5) around zero:

$$P(x) \approx \frac{3a - 2b}{2\varepsilon} + \frac{6b - 5a}{4\varepsilon^3}x^2 + O(x^4), \quad (6)$$

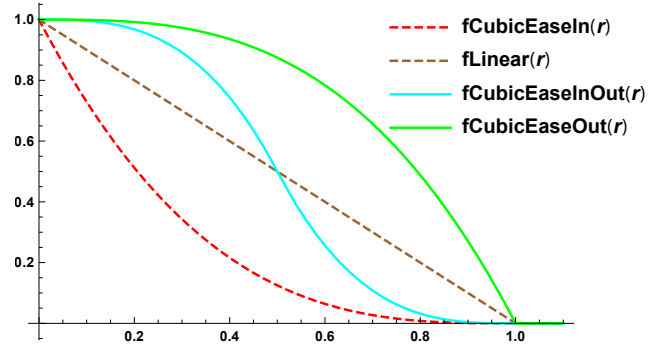


Figure 4: Examples of radially symmetric falloff profiles for a typical displacement brush of the form $\mathbf{u}(\mathbf{r}) = P(r) \mathbf{u}_0$. None of these correspond to physical elasticity solutions, but they exhibit the need for artistic control of the smoothness amount, since the dashed profiles present a cusp due to the non-zero radial derivative at $r = 0$.

which exhibits a smooth parabolic shape. An exception is the classical Kelvin's solution [Kelvin 1848] (corresponding to \mathbf{u}_ε with $\varepsilon = 0$), which is singular and returns infinite at the brush tip. Next, we describe how to combine Kelvinlets of multiple regularization scales in order to modulate the falloff profile.

5.1 Multi-scale Convolutions

We propose to introduce cusps by convolving the Kelvinlet solution \mathbf{u}_ε against a multi-scale distribution $\eta(\varepsilon; \varepsilon_0)$ of radial scale values ε . This distribution η is chosen by ensuring a series of properties:

- (1) η must be nonnegative and normalized such that

$$\int_0^\infty \eta(\varepsilon; \varepsilon_0) d\varepsilon = 1; \quad (7)$$

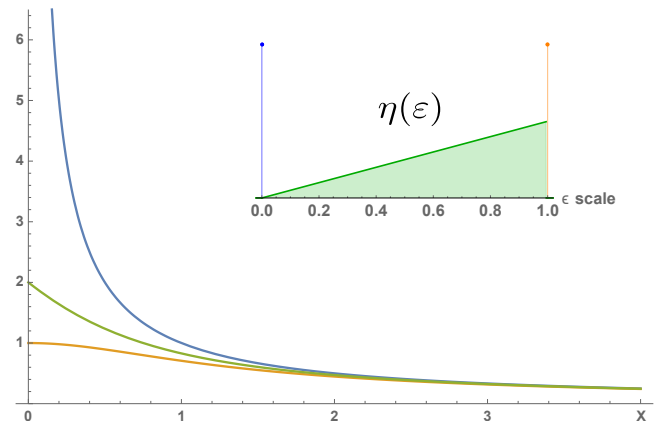


Figure 5: Comparison of Kelvinlet falloff profiles $P(x)$ convolved with different scale density functions $\eta(\varepsilon)$ (shown inset): (Orange) the smooth Kelvinlet solution corresponds to a multi-scale convolution with a single-scale Dirac density function, e.g., here $\varepsilon=1$ so $\eta(\varepsilon) = \delta(\varepsilon-1)$; (Blue) Kelvin's classical singular solution ($\varepsilon=0$) corresponds to $\eta(\varepsilon) = \delta(\varepsilon)$; (Green) the Cusped Kelvinlet is a multi-scale convolution with a piecewise linear η function. Note that they all have a similar $O(1/x)$ far-field decay, but differ near $x=0$.

- (2) $\eta(0; \epsilon_0) = 0$ so that the singular Kelvinlet is eliminated and the resulting displacement is finite at the origin;
- (3) $\eta(\epsilon; \epsilon_0) = 0$ for every $\epsilon \geq \epsilon_0$, so that the largest radial scale is well defined;
- (4) the resulting falloff profile $P(x)$ must be monotonic, non-negative, and discontinuous at the origin.

Given a distribution η verifying the properties above, we then define the ϵ -convolved Kelvinlet matrix as:

$$\int_0^\infty \mathcal{K}_\epsilon(\mathbf{r}) \eta(\epsilon; \epsilon_0) d\epsilon. \quad (8)$$

Since it is a linear superposition of solutions of the Navier-Cauchy equation, this convolved Kelvinlet is also a solution of linear elastostatics, associated with a convolution of regularized force loads.

Although various basis function are feasible, we observed in our derivation that is sufficient to model $\eta(\epsilon; \epsilon_0)$ using a monomial distribution of degree n :

$$\eta(\epsilon; \epsilon_0) \equiv \eta(\epsilon; \epsilon_0, n) = \begin{cases} \frac{(n+1)}{\epsilon_0^{n+1}} \epsilon^n & \epsilon \leq \epsilon_0 \\ 0 & \text{otherwise.} \end{cases} \quad (9)$$

We are now ready to compute cusped solutions by evaluating the ϵ -convolved Kelvinlet matrix analytically.

5.2 Analytical Solution

The integral in (8) with monomial distributions can be computed using symbolic packages (e.g., Mathematica), but yields a long expression with many hypergeometric functions and complex dependence on n . Instead, we considered series expansions of the profile function $P(x) \equiv K_\epsilon^{xx}(x, 0, 0)$ about $x = 0_+$ to determine the monomial degree n that produces a cusp. We found that a cusped deformation satisfying the required conditions listed in §5.1 can be obtained with $n = 1$. Using the canonical form in (2), the cusped Kelvinlet is

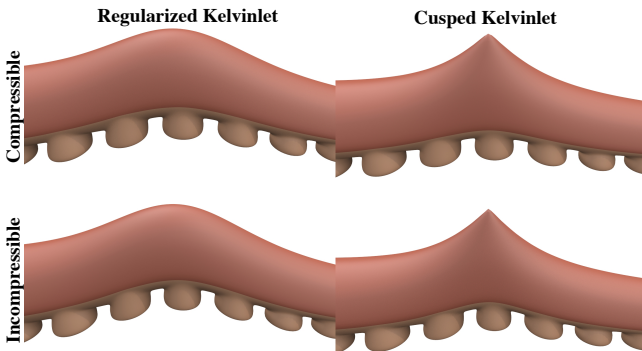


Figure 6: 3D Cusped Kelvinlet provides additional sharpness (derivative control) compared to the traditional regularized Kelvinlet solution: (Top) compressible ($\nu = 0$) and (Bottom) incompressible ($\nu = 1/2$) materials. All results use the same brush scale, ϵ , and vertical displacement. ©Disney/Pixar

then expressed in closed-form with the radial coefficients:

$$\begin{cases} A_\epsilon(r) = \frac{a}{\epsilon^2} \left(\frac{r^2}{r_\epsilon} + 3r_\epsilon - 4r \right) + \frac{2b}{\epsilon^2} (r - r_\epsilon) \\ B_\epsilon(r) = \frac{2b}{\epsilon^2} \left(\frac{1}{r} - \frac{1}{r_\epsilon} \right). \end{cases} \quad (10)$$

The corresponding falloff profile is

$$P(x) = \frac{\epsilon^2(3a - 2b) + 4x^2(a - b)}{\epsilon^2 x_\epsilon} - \frac{4(a - b)}{\epsilon^2} |x|. \quad (11)$$

Expanding the profile near zero (i.e., $|x| \ll \epsilon$) yields

$$P(x) \approx \frac{3a - 2b}{\epsilon} - \frac{4(a - b)}{\epsilon^2} |x| + \frac{(5a - 6b)}{2\epsilon^3} x^2 + O(x^4), \quad (12)$$

which has a clear cusp-like structure due to the $|x|$ term for every material configuration so that $a \neq b$. We note that the special case of $a = b$ requires a non-physical Poisson's ratio $\nu = 3/4$ and therefore can be disregarded. Observe that the falloff profile produced by a cusped Kelvinlet still exhibits an $O(1/r)$ far-field decay:

$$P(x) \approx \frac{a}{x} - \frac{b\epsilon^2}{2x^3} + O(1/x^5), \quad (13)$$

thus matching the regularized Kelvinlet solution as $x \rightarrow \infty$ (Figure 5). One can further create localized cusped solutions by combining cusped Kelvinlets of multiple scales ϵ via multi-scale extrapolation, as previously described in [de Goes and James 2017]. However, there is a more effective way to obtain cusped solutions with fast decay rates for which multi-scale extrapolation can be avoided entirely. To this end, we must first introduce Laplacian Kelvinlets in the following section.

6 LAPLACIAN LOCALIZATION

Prior work on Kelvinlets relied on multi-scale extrapolation to produce faster decay by linearly combining regularized solutions of different scales ϵ so that the leading $1/r$ terms in a far-field expansion were annihilated. It turns out that fast decay can be achieved analytically, without combining multiple solutions, by repeated application of the Laplacian operator. Since Navier's operator \mathbf{N} commutes with the Laplacian Δ , it follows that Laplacians of Kelvinlets (and their derivatives) are also solutions to Navier-Cauchy equation, with suitably differentiated force distributions, i.e.:

$$\mathbf{N} \Delta^m \mathbf{u}_\epsilon(\mathbf{r}) = \Delta^m \mathbf{N} \mathbf{u}_\epsilon(\mathbf{r}) = \Delta^m \mathbf{b}_\epsilon(\mathbf{r}), \quad m = 0, 1, 2, \dots \quad (14)$$

We further notice that these differentiated Kelvinlets have faster far-field decay, while also retaining a similar volume response. Plots of Laplacian Kelvinlets are shown in Figure 7, and the corresponding force densities $\rho_\epsilon(r)$ are given in Figure 8.

We therefore compute the Laplacian of the regularized Kelvinlet and obtain a new solution referred to as *Laplacian Kelvinlet*, which can be expressed analytically using the canonical coefficients

$$A_\epsilon(r) = \frac{15a\epsilon^4 - 2br_\epsilon^2(5\epsilon^2 + 2r^2)}{2r_\epsilon^7}, \quad B_\epsilon(r) = \frac{3b(7\epsilon^2 + 2r^2)}{r_\epsilon^7}. \quad (15)$$

This solution decays as $O(1/r^3)$ and is the analogue of the bi-scale Kelvinlet [de Goes and James 2017].

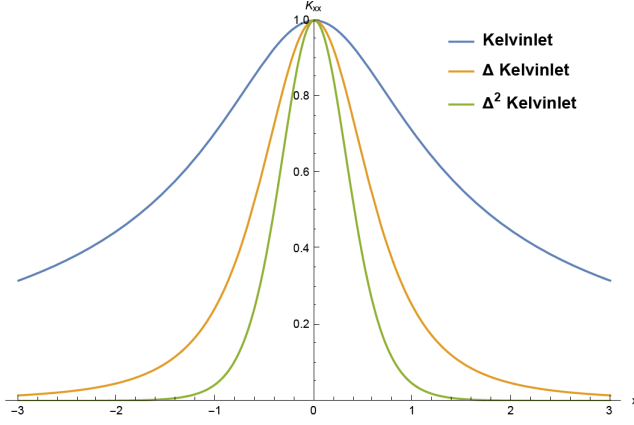


Figure 7: Laplacian Kelvinlets provide compact analytical expressions for elastic deformations with fast decay. This plot exhibits solutions normalized to one at the origin with $a = 1$, $b = 1/2$, and $\varepsilon = 1$.

Similarly, we can derive the *Bi-Laplacian Kelvinlet*, which yields another compact expression for the radial coefficients

$$A_\varepsilon(r) = \frac{105\varepsilon^4 (3a(\varepsilon^2 - 2r^2) - 2br_\varepsilon^2)}{2r_\varepsilon^{11}}, \quad B_\varepsilon(r) = \frac{945b\varepsilon^4}{r_\varepsilon^{11}}. \quad (16)$$

Although this solution is the analogue of the $O(1/r^5)$ tri-scale Kelvinlet [de Goes and James 2017], it decays surprisingly far faster as $O(1/r^9)$, which was previously only achievable with a costly five-scale extrapolation scheme.

We finally point out that higher-order Laplacian Kelvinlets are possible, but seem unnecessary given the extremely fast decay of the Bi-Laplacian Kelvinlets, and undesirable due to the possible introduction of numerical issues associated with cancellation and division by high-orders powers of r_ε . Affine Laplacian Kelvinlets are also straightforward to derive following the gradient-based construction in [de Goes and James 2017]. However, since gradients of cusped solutions are discontinuous at the origin, they are not desirable in practice. Therefore, we limit our Laplacian localized and cusped solutions only for grab-like brush interactions. Lastly, we present the 2D version of these solutions in Appendix A.

7 SHARP KELVINLETS

Equipped with multi-scale convolution and the Laplacian machinery, we can now report the complete family of cusped elastic deformations with varying degrees of localization, which we refer to as *Sharp Kelvinlets*. To combine the cusped formulation with a specific Laplacian Kelvinlet, we repeated the steps described in §5.2 and manually searched for the monomial degree n of the scale distribution $\eta(\varepsilon; \varepsilon_0, n)$ that leads to a cusped profile function. In practice, we noticed that the results followed a simple pattern that increases n by one for every Laplacian differentiation.

The *cusped Laplacian Kelvinlet*, for instance, can be generated by integrating $\Delta \mathcal{K}_\varepsilon$ against a monomial distribution $\eta(\varepsilon; \varepsilon_0, n)$ with $n = 3$. The resulting closed-form solution has a fast $O(1/r^3)$ falloff

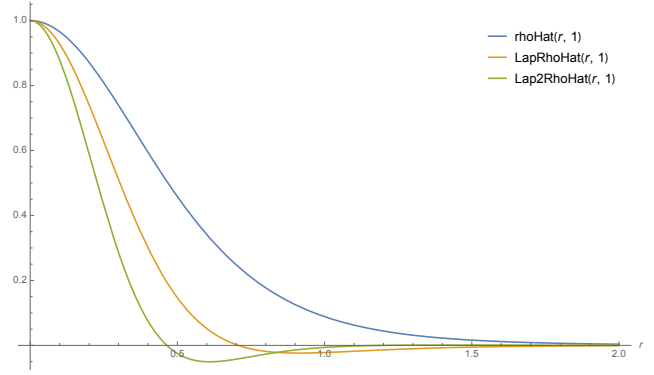


Figure 8: Force densities $\rho_\varepsilon(r)$ of Laplacian Kelvinlets exhibit negative lobes due to Laplacian differentiation, which act as “shields” that localize the displacement response. In this plot, the number of applied Laplacian operators equals the number of roots of the density. The densities are also normalized to one at the origin.

produced by the following radial coefficients:

$$\left\{ \begin{array}{l} A_\varepsilon(r) = \frac{2}{\varepsilon^4 r_\varepsilon^5} \left[(15a - 10b)\varepsilon^6 + (90a - 88b)\varepsilon^4 r^2 \right. \\ \quad \left. + 120\varepsilon^2 r^4 (a - b) + 48(a - b)r(r^5 - r_\varepsilon^5) \right] \\ B_\varepsilon(r) = \frac{-12b}{\varepsilon^4 r r_\varepsilon^5} \left[2\varepsilon^2 r^2 (4r_\varepsilon - 5r) + 4r^4 (r_\varepsilon - r) \right. \\ \quad \left. + \varepsilon^4 (4r_\varepsilon - 7r) \right]. \end{array} \right. \quad (17)$$

Similarly, the *cusped Bi-Laplacian Kelvinlet* is found for $n = 5$ and has a super-fast $O(1/r^9)$ decay rate as $r \rightarrow \infty$, making it highly suitable for detailed sculpting and editing work (Figure 9).

The raw expression for its radial coefficients is quite long and requires care to evaluate. Instead, we rearrange these analytical expressions in a form more convenient for computation. To do so, we rescale r to be in units of ε by setting $r = \varepsilon R$, and then we carefully factored the Kelvinlet solution into subexpressions in terms of R , yielding:

$$\left\{ \begin{array}{l} A_\varepsilon(r) = \frac{9}{\varepsilon^5 R_1^{10}} \left\{ a \left[-512 R R_1^{10} + (((((512 R^2 + 2304) R^2 \right. \right. \right. \\ \quad \left. \left. \left. + 4032) R^2 + 3360) R^2 + 1260) R^2 + 105) R_1 \right] \right. \\ \quad \left. + 2b \left[128 R R_1^{10} - R_1^3 (35 + R^2 (280 \right. \right. \right. \\ \quad \left. \left. \left. + R^2 (560 + R^2 (448 + 128 R^2)))) \right] \right\} \\ B_\varepsilon(r) = \frac{18b}{\varepsilon^7 R R_1^9} \left[128 R_1^9 - R (R^2 (R^2 (R^2 (128 R^2 + 576) \right. \right. \right. \\ \quad \left. \left. \left. + 1008) + 840) + 315) \right], \end{array} \right. \quad (18)$$

where $R_1 \equiv \sqrt{R^2 + 1}$. We also observed that the a and $2b$ coefficients (in square brackets) are a source of catastrophic cancellation effects for large R . In practice, this cancellation implies that the solution is numerically zero starting at $R = 5$ (Figure 10) and it can be problematic in single-precision arithmetics. Therefore, we evaluate these expressions only for $R < 5$, otherwise we return zero.

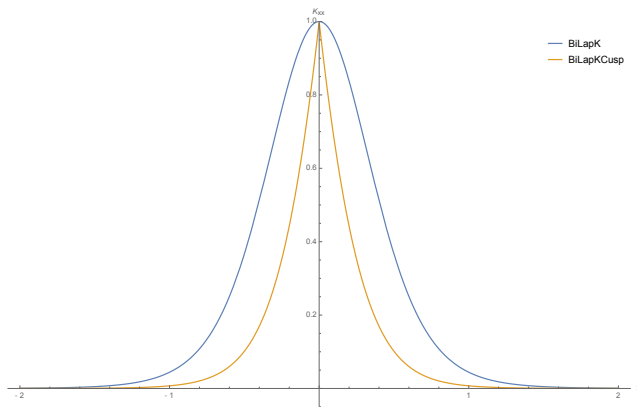


Figure 9: Bi-Laplacian Kelvinlet and its cusped solution shown for the K_ϵ^{xx} component with $\epsilon=1$. Both exhibit a rapid $O(1/r^9)$ falloff, but with different sharpness near the brush origin. We can also blend these two solutions linearly for fine falloff control.

8 RESULTS

We implemented Sharp Kelvinlets as a C++ plugin to the sculpting package of Pixar animation system (Presto), to Maya, and Houdini. The deformation is computed by evaluating the Kelvinlet displacement for every selected point in parallel via Intel TBB. The user can also edit the falloff sharpness and locality interactively, in addition to the brush scale ϵ . Similar to [de Goes and James 2017], we observed performances averaging near 60 frames per second on a 2.3 GHz Intel Xeon E5-2699 with 18 cores for scenes with 100k points. In the supplemental material, we provide a reference C++ implementation that includes Sharp Kelvinlets as well as affine [de Goes and James 2017] and dynamic Kelvinlets [de Goes and James 2018]. Finally, results for 2D Laplacian and Cusp Kelvinlets are listed in Appendix A.

Figure 11 showcases the falloff control offered by Sharp Kelvinlets. Figure 1 compares the deformation generated by three Kelvinlets applied simultaneously on a tentacle model with various levels of spikyness and locality. In Figure 2, we include a few frames of an animation sequence from *Incredibles 2* sculpted using a combination Kelvinlet brushes. Our tool was also employed as flex rig deformer, which are illustrated in Figure 3 and in the supplemental video.

It is worth noticing that Sharp Kelvinlets exhibit the same limitations from previous Kelvinlet techniques. In particular, surfaces deformed using Kelvinlets move as if embedded in an infinite medium. As a result, points that are spatially close but geodesically apart will move together. To address these issues, our implementation also supports surface-based masking, which rescales the Kelvinlet displacements in a post-processing step.

9 CONCLUSION

In this work, we conveyed new extensions of the regularized Kelvinlets solutions for volume sculpting based on elasticity. Motivated by earliest feedback received when we deployed Kelvinlets at Pixar, we introduced a family of *Sharp Kelvinlet* solutions for analytical and efficient evaluation of localized and cusped Kelvinlet brushes suited to non-smooth, spiky edits. Laplacian localization was also

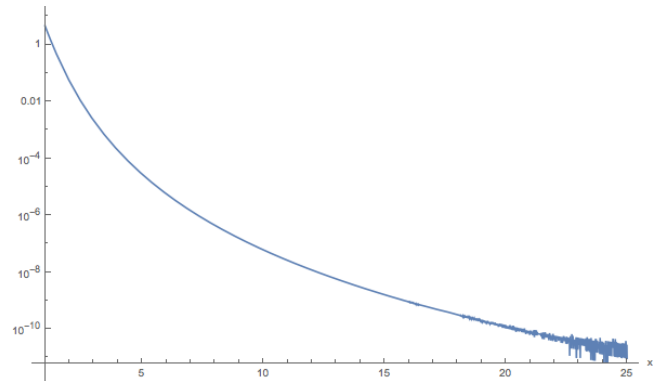


Figure 10: Catastrophic cancellation can result when evaluating the cusped Bi-Laplacian Kelvinlet (shown for the K_ϵ^{xx} component with $\epsilon=1$) for large r values, which can limit precision in finite precision arithmetic (see oscillations in the right side of the plot). Fortunately, it does not need to be evaluated for large values (e.g., beyond $r=10\epsilon$) since it rapidly approaches zero due to its rapid $O(1/r^9)$ falloff.

utilized to construct Kelvinlet solutions with increasingly fast far-field decay. Finally, we note that artists can blend between smooth and cusped solutions interactively, thus achieving a variety of brush profiles for sculpting or other production applications.

ACKNOWLEDGMENTS

We would like to thank Alonso Martinez for the Jack-Jack sequence and Mark Piretti for rigging examples.

REFERENCES

- Alexis Angelidis, Marie-Paule Cani, Geoff Wyvill, and Scott King. 2006. Swirling-Sweepers: Constant volume modeling. *Graph. Models* 68, 4 (2006), 324–332.
- Alexis Angelidis, Geoff Wyvill, and Marie-Paule Cani. 2004. Sweepers: Swept user-defined tools for modeling by deformation. In *Proc. of Shape Modeling Applications*. IEEE, 63–73.
- Fernando de Goes and Doug L. James. 2017. Regularized Kelvinlets: Sculpting Brushes Based on Fundamental Solutions of Elasticity. *ACM Trans. Graph.* 36, 4, Article 40 (2017), 11 pages.
- Fernando de Goes and Doug L. James. 2018. Dynamic Kelvinlets: Secondary Motions Based on Fundamental Solutions of Elastodynamics. *ACM Trans. Graph.* 37, 4, Article 81 (2018), 10 pages.
- Lou Hamou-Lhadj, Rich Hurrey, Salvatore Melluso, Mark Piretti, Kevin Singleton, Jacob Spiers, and Nancy Tsang. 2018. Reinterpreting Memorable Characters in *Incredibles 2*. In *ACM SIGGRAPH 2018 Talks*. Article 47, 2 pages.
- David Iron, Michael J Ward, and Juncheng Wei. 2001. The stability of spike solutions to the one-dimensional Gierer–Meinhardt model. *Physica D: Nonlinear Phenomena* 150, 1-2 (2001), 25–62.
- Riei Ishizeki and Martin Kruczenski. 2007. Single spike solutions for strings on S 2 and S 3. *Physical Review D* 76, 12 (2007), 126006.
- Lord Kelvin. 1848. Note on the integration of the equations of equilibrium of an elastic solid. *Cambridge and Dublin Mathematical Journal* 3 (1848), 87–89.
- Zhijun Qiao and Xin Brian Qiao. 2005. Cusp solitons and cusp-like singular solutions for nonlinear equations. *Chaos, Solitons & Fractals* 25, 1 (2005), 153–163.
- William S. Slaughter. 2002. *The Linearized Theory of Elasticity*. Birkhäuser Basel.
- Ian N Sneddon. 1965. The relation between load and penetration in the axisymmetric Boussinesq problem for a punch of arbitrary profile. *International Journal of Engineering Science* 3, 1 (1965), 47–57.
- Jon Sparring, Mads Nielsen, Luc Florack, and Peter Johansen. 2013. *Gaussian scale-space theory*. Vol. 8. Springer Science & Business Media.
- Peter Tieryas, Henry Garcia, Stacey Truman, and Evan Bonifacio. 2017. Bringing Lou to Life: A Study in Creating Lou. In *ACM SIGGRAPH 2017 Talks*. ACM, Article 1, 2 pages.
- Wolfram von Funck, Holger Theisel, and Hans-Peter Seidel. 2006. Vector field based shape deformations. *ACM Trans. on Graph.* 25, 3 (2006), 1118–1125.
- Andrew P. Witkin. 1983. Scale-Space Filtering. In *IJCAI*.

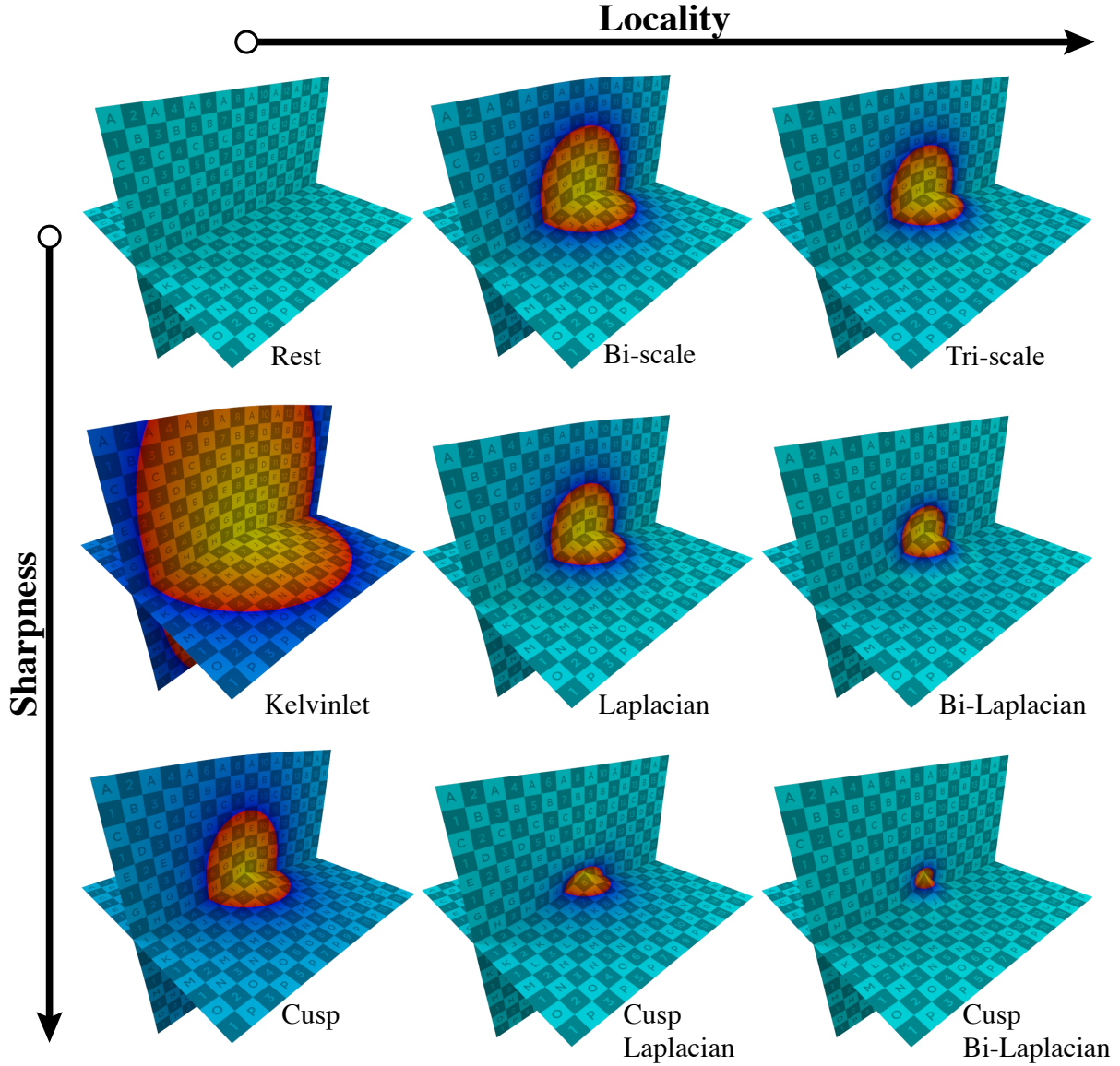


Figure 11: Comparison of all 3D Kelvinlet brushes: Colors indicate the displacement magnitude; $\nu = 1/2$, the same ϵ and the same brush displacement of $(0,1,0)$ for all examples. The blue-red discontinuity represents magnitude of $1/2$.

A SHARP KELVINLETS IN 2D

We now report the 2D Laplacian Kelvinlet and Cusp solutions, following a process analogous to the 3D results shown earlier in the paper. All 2D solutions are of the standard form

$$K(\mathbf{r}) = A(r)\mathbf{I} + B(r)\mathbf{r}\mathbf{r}^t, \tag{19}$$

for which we now report the resulting $A(r)$ and $B(r)$ functions; here $\mathbf{r} = [x, y]$, $r = \|\mathbf{r}\|$, and $r_\epsilon = \sqrt{r^2 + \epsilon^2}$.

A.1 2D Laplacian Kelvinlets

The 2D Laplacian Kelvinlets results are reported below, and plotted in Figure 12. The 2D regularized Kelvinlet is known from [de Goes

and James 2017]:

$$A_\epsilon(r) = 2(b-a)\ln(r_\epsilon) + a\frac{\epsilon^2}{r_\epsilon^2}, \quad B_\epsilon(r) = \frac{2b}{r_\epsilon^2} \tag{20}$$

and can be derived by suitably integrating the 3D Kelvinlet. It has a nonzero far-field displacement due to the $O(\log(r_\epsilon))$ decay.

2D Laplacian Kelvinlet: The negative Laplacian of (20) yields

$$A_\epsilon(r) = \frac{4(2a\epsilon^4 - b(2\epsilon^4 + 3\epsilon^2r^2 + r^4))}{r_\epsilon^6} \tag{21}$$

$$B_\epsilon(r) = \frac{8b(3\epsilon^2 + r^2)}{r_\epsilon^6}$$

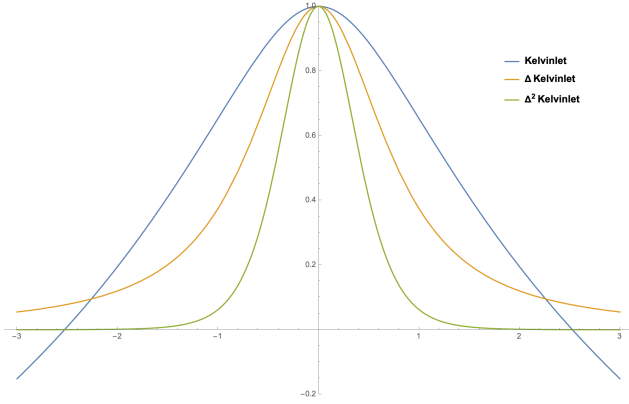


Figure 12: 2D Laplacian Kelvinlet Profiles ($P(x) = \mathcal{K}_{xx}(x, 0)$) also exhibit fast decay with repeated Laplacian differentiation. (The solutions are normalized to 1 at the origin; $a = 1$, $b = 1/2$, $\varepsilon = 1$.)

which has a faster $O(1/r^2)$ decay rate.

2D Bi-Laplacian Kelvinlet: This solution is

$$\begin{aligned} A_\varepsilon(r) &= \frac{96\varepsilon^4 (a(\varepsilon^2 - 3r^2) - b(\varepsilon^2 + r^2))}{r_\varepsilon^{10}}, \\ B_\varepsilon(r) &= \frac{768b\varepsilon^4}{r_\varepsilon^{10}} \end{aligned} \quad (22)$$

which has a much faster far-field decay rate of $O(1/r^8)$, analogous to the 3D Bi-Laplacian Kelvinlet's steep decay.

A.2 2D Sharp Kelvinlets

Similar to the 3D case, the multiscale convolution with 2D (Laplacian) Kelvinlets produces cusp solutions, but with n shifted down by 1. All 2D cusp Kelvinlet solutions are expressible in 2D standard form (19), for which we now report the resulting $A(r)$ and $B(r)$ functions. Notice the presence of log and arctan functions.

2D Cusped Kelvinlet is obtained for $n = 0$:

$$\begin{aligned} A_\varepsilon(r) &= 2(b - a) \log r_\varepsilon + (2b - 3a) \left(\frac{r}{\varepsilon} \tan^{-1} \left(\frac{\varepsilon}{r} \right) - 1 \right) \\ B_\varepsilon(r) &= \frac{2b \tan^{-1} \left(\frac{\varepsilon}{r} \right)}{\varepsilon r} \end{aligned} \quad (23)$$

Similar to the 2D Kelvinlet, the 2D Cusped Kelvinlet is not localized due to the $\log r_\varepsilon$ far-field form of its profile

$$P(x) \approx 2(b + (b - a) \log x) - \frac{b\varepsilon^2}{3x^2} + O\left(\frac{1}{x^4}\right), \quad x \rightarrow \infty. \quad (24)$$

2D Cusped Laplacian Kelvinlet is obtained for $n = 2$:

$$\begin{aligned} A_\varepsilon(r) &= \frac{3}{\varepsilon^3} \left(\frac{\varepsilon^3(5a - 2b)}{r_\varepsilon^2} + 5(3a - 2b)(r \tan^{-1}(\varepsilon/r) - \varepsilon) \right. \\ &\quad \left. + \frac{2a\varepsilon^5}{r_\varepsilon^4} \right) \\ B_\varepsilon(r) &= \frac{6b}{\varepsilon^3} \left(\frac{7\varepsilon^3 + 5\varepsilon r^2}{r_\varepsilon^4} - \frac{5 \tan^{-1} \left(\frac{\varepsilon}{r} \right)}{r} \right) \end{aligned} \quad (25)$$

Its profile's far-field form is $P(x) \approx -4b/x^2$.

2D Cusped Bi-Laplacian Kelvinlet requires $n = 4$:

$$\begin{aligned} A_\varepsilon(r) &= \frac{5}{\varepsilon^5 r_\varepsilon^8} \left(96(a - b)\varepsilon^9 + r(3a - 2b) \left(279\varepsilon^7 r \right. \right. \\ &\quad \left. \left. + 511\varepsilon^5 r^3 + 385\varepsilon^3 r^5 + 105\varepsilon r^7 - 105r_\varepsilon^8 \tan^{-1}(\varepsilon/r) \right) \right) \\ B_\varepsilon(r) &= \frac{10b}{\varepsilon^5} \left(\frac{105 \tan^{-1}(\varepsilon/r)}{r} \right. \\ &\quad \left. - \frac{\varepsilon (279\varepsilon^6 + 511\varepsilon^4 r^2 + 385\varepsilon^2 r^4 + 105r^6)}{r_\varepsilon^8} \right) \end{aligned} \quad (26)$$

This cusp solution exhibits an extremely rapid $1/r^8$ far-field decay, making it ideal for detailed cusp edits. Its profile's far-field form is $P(x) \approx \frac{160}{3}(7b - 3a)\frac{\varepsilon^4}{x^8}$.